**One-sentence summary:** Increased glycolytic stress in cancer cells stimulates p53 production to maintain metabolic homeostasis.

**Editor's summary:**
**Protective p53 response**
To fuel their rapid proliferation, tumor cells increase their rates of glycolysis, which generates precursors for biosynthetic pathways, but also results in an increase in the NADH:$NAD^+$ ratio. Birts *et al*. found that, in highly glycolytic cancer cells in vitro, the increased NADH:$NAD^+$ ratio resulted in an increase in the abundance of the NADH-bound forms of CtBP family transcriptional regulators, which prevented their interaction with the p53-binding protein HDM2, thus enabling the accumulation of p53. The resulting expression of p53 target genes was required to maintain metabolic homeostasis, highlighting a role for p53 in protecting cells from glycolytic stress.

# p53 is regulated by aerobic glycolysis in cancer cells by the CtBP family of NADH-dependent transcriptional regulators

Charles N. Birts[1,2], Arindam Banerjee[1], Matthew Darley[1], Charles R. Dunlop[1], Sarah Nelson[1], Sharandip K. Nijjar[3], Rachel Parker[1], Jonathan West[1,2] Ali Tavassoli[2,3], Matthew J.J. Rose-Zerilli[1,2] Jeremy P. Blaydes[1,2*]

[1]Cancer Sciences Unit, Faculty of Medicine, University of Southampton, SO16 6YD, UK. [2]Institute for Life Sciences, University of Southampton, SO17 1BJ, UK. [3]Chemistry, University of Southampton, SO17 1BJ, UK.

[*]Corresponding author. Email: j.p.blaydes@soton.ac.uk

## ABSTRACT

High rates of glycolysis in cancer cells are a well-established characteristic of many human tumors, providing rapidly proliferating cancer cells with metabolites that can be used as precursors for anabolic pathways. Maintenance of high glycolytic rates depends upon the lactate dehydrogenase–catalyzed regeneration of $NAD^+$ from GAPDH-generated NADH, because an increased NADH:$NAD^+$ ratio inhibits GAPDH. Here, using human breast cancer cell models, we identified a pathway in which changes in the extra-mitochondrial free NADH:$NAD^+$ ratio signaled through the CtBP family of NADH-sensitive transcriptional regulators to control the abundance and activity of p53. NADH-free forms of CtBPs cooperated with the p53-binding partner HDM2 to suppress p53 function, and loss of these forms in highly glycolytic cells resulted in p53 accumulation. We propose that this pathway represents a "glycolytic stress response" in which the initiation of a protective p53 response by an increased NADH:$NAD^+$ ratio enables cells to avoid cellular damage caused by mismatches between metabolic supply and demand.

## INTRODUCTION

Constitutive aerobic glycolysis ("The Warburg Effect") (*1*) is a hallmark of cancer cells that is commonly caused by mutations in oncogenes and tumor-suppressor genes (*2*). It has multiple consequences for tumor cells (*2*), including the ability to generate ATP, which decreases reliance on oxygen for ATP generation, thus reducing the generation of potentially damaging reactive oxygen species (ROS) by the mitochondrial electron transport chain. Through the provision of glucose-6 phosphate for the oxidative pentose phosphate pathway, glycolysis also facilitates the generation of NADPH, which provides reducing equivalents for ROS-protective pathways (*3*). Glycolytic intermediates are also important precursors for anabolic pathways involved in DNA,

lipid, and protein synthesis (*4*). The final steps of glycolysis, which generate both ATP and precursors for serine and nucleotide biosynthesis, are dependent on glyceraldehyde-3-phosphate dehydrogenase (GAPDH) (*5*). GAPDH is in turn dependent on the coenzyme $NAD^+$, which it reduces to NADH. To sustain GAPDH activity, a low extra-mitochondrial free NADH:$NAD^+$ ratio is maintained by oxidation of NADH to $NAD^+$ by the mitochondrial electron transport chain and, in highly glycolytic cells, lactate dehydrogenase (LDH). Cellular export of the LDH-generated lactate is facilitated by the monocarboxylic acid transporters MCT1 and MCT4 (*6*). Despite these compensatory mechanisms, an increase in the NADH:$NAD^+$ ratio occurs under physiological and pathophysiological conditions where the rate of glycolytic flux though GAPDH is not fully matched by the cells' ability to regenerate $NAD^+$; for example, under hypoxia the NADH:$NAD^+$ ratio increases more than three-fold (*7*). Differences between nontransformed cells and tumor cells are comparable (*8*), and the ratio is consistently increased in cancer cells exhibiting The Warburg Effect (*8-10*). This ratio is also increased by lactate (*11*), enhanced production of which is a defining feature of The Warburg Effect (*1, 2*), and which accumulates in the tumor microenvironment to concentrations that have profound effects on cancer cell phenotype (*12, 13*). A clear demonstration that the flux of intermediates from the later stages of glycolysis into anabolic pathways can be rate-limiting for cancer development is the genomic amplification and over-expression of the *PHGDH* gene, which encodes phosphoglycerate dehydrogenase, in breast cancer and melanoma, diverting glycolytic carbon into serine and glycine metabolism (*14, 15*). Furthermore, novel anti-cancer strategies that aim to target glycolytic cells by inhibiting either LDH or MCT1/2/4-mediated lactate export (*2, 16-19*), further increase the extra-mitochondrial free NADH:$NAD^+$ ratio, with consequent negative effects on GAPDH-dependent glycolysis.

An important consequence of the inability of an anabolically active cell to maintain the NADH:$NAD^+$ ratio at the low levels required for rapid glycolysis is an increased likelihood that the cell will be unable to appropriately match its supply of metabolites with its high metabolic demands, a scenario that we have termed "glycolytic stress." Such a mismatch may result in increased ROS production due to the excessive channeling of pyruvate into the mitochondrial TCA cycle and electron transport chain (*16*), or nucleotide depletion due to reduced amounts of glycolytic intermediates, such as 3-phosphoglycerate, that are required for anabolic pathways (*20, 21*). These effects may cause DNA damage, potentially leading to either cell death, or the survival of cells with acquired genetic mutations. We therefore speculated about the existence of a stress-response pathway able to detect such glycolytic stress, which prevents such damage by rebalancing metabolic demand with metabolic capacity. The multi-stress–responsive transcription factor p53 (*22, 23*) is a strong candidate for an effector in such a pathway, because it induces a program of gene expression that matches the requirements of such an effector. First, this transcriptional program reduces metabolic demand by inhibiting cell proliferation and suppressing anabolic metabolism, thus minimizing the likelihood that glycolytic stress will result in cellular damage. Second, genes induced by p53 direct cellular metabolism away from GAPDH-dependent glycolysis into pathways that protect from ROS, notably the *TIGAR*-dependent suppression of phosphofructokinase 1 (PFK-1). This suppression of PFK-1 diverts metabolites into the pentose phosphate pathway and also promotes ATP synthesis by increasing fatty acid oxidation and mitochondrial oxidative phosphorylation (OXPHOS) (*3, 24-26*). Consistent with a role in metabolic homeostasis, p53 regulates the cellular response to energy stress, serine restriction, and NADPH metabolism (*27-29*). Furthermore, in a study of tumor material from breast cancer patients, wild-type p53 gene status correlated with a lactic acidosis–induced gene signature (*30*), further

supporting a role for p53 in directing a glycolytic stress–dependent transcriptional response in vivo. Whereas increased amounts of tumor lactate can be associated with poor clinical outcome, the presence of a lactic acidosis–induced gene signature is associated with favorable outcome (*30*), which is consistent with a potential role of this response in the prevention of metabolic imbalance–related genetic damage.

The extra-mitochondrial free NADH:$NAD^+$ ratio represents a potential signal for such glycolytic stress. The ratio in nonmalignant cells is ~1:700 (*7, 31*) and thus after a typical ~three-fold change in the ratio induced by hypoxia or transformation (*7, 8*), it is only the concentration of NADH that changes sufficiently to act as such a signal (*31*). Two proteins are described as both NADH sensors and p53 regulators: NAD(P)H quinone dehydrogenase 1 (NQO1) and C-terminal binding proteins (CtBPs). The mechanism of p53 regulation by NQO1 is well studied (*32*), but NQO1 does not distinguish between NADH and NADPH [free extra-mitochondrial concentrations of NADPH exceed that of NADH by about four-fold (*33*)]. The CtBP proteins (CtBP1 and CtBP2) are near-ubiquitous transcriptional regulators, which are sensitive to NADH but not NADPH (*34, 35*). Binding of NADH toggles CtBPs between monomeric ($NADH^{free}$) and dimeric ($NADH^{bound}$) forms, as well as controlling their differential binding to cellular partner proteins (*31, 36-40*). The $K_D$ of NADH for CtBP is ~100 nM (approximately equal to the extra-mitochondrial free NADH concentration), whereas the $K_D$ of $NAD^+$ is >100-fold greater (*31*). These biochemical studies predict that metabolic alterations that increase the NADH:$NAD^+$ ratio will increase CtBP dimerization and induce a CtBP-dependent phenotypic response; cancer cell biology studies from multiple independent laboratories are entirely consistent with this hypothesis (*7, 41, 42*). We have

previously shown that, when overexpressed, NADH-free (monomeric) forms of CtBPs can bind to the p53 regulator HDM2 [human form of murine double minute-2 (MDM2)] to suppress p53 function (*43*), and that siRNA-mediated CtBP knockdown induces p53 protein accumulation (*44*). We have now undertaken further experiments to define the role of this pathway in the response to glycolytic stress.

## RESULTS

### p53 abundance and activity in proliferating cells are increased by high rates of glycolysis

To determine how high rates of aerobic glycolysis in cancer cells affect p53, it was necessary to generate matched pairs of cell lines that proliferated normally but differed in their glycolytic states. Starting with a highly glycolytic cancer cell line and completely removing glucose from the medium results in ATP depletion and the activation of an AMP/AMPK-dependent p53 response (*28*). Similarly, it is not possible to merely reduce the glucose concentration in the culture medium to an extent that would restrict glycolysis, because the cells then rapidly deplete the glucose concentration towards zero (*45*), unless complex flow cell systems are used to overcome this problem (*46*). We have thus used the approach of culturing cells in medium containing an alternative sugar, in this case fructose, which is imported into cells less rapidly than is glucose, but is still metabolized by glycolysis. Once cells have adapted their metabolism in response to this reduced intracellular sugar availability, this model enables cell cultures with stable low rates of glycolysis to be established (*45*, *47*, *48*). Three different breast cancer cell lines, MCF-7 cells and

ZR-75-1 cells (both of which have wild-type p53) and MDA-MB-231 cells (which express a functionally compromised mutant p53), were used for this current study.

When MCF-7 cells, which are normally cultured in DMEM containing standard 25 mM glucose (MCF-$7^{GLU}$ cells), was cultured in medium in which glucose was either lacking or replaced with 10 mM fructose, proliferation was markedly decreased (Fig. 1A). However, after adaptation to culture with fructose for 30 days (MCF-$7^{FRU}$ cells), proliferation rates were equal to, or greater than, those of MCF-$7^{GLU}$ cultures (Fig. 1A). Comparable results were obtained with ZR-75-1 cells (which also express wild-type p53) and MDA-MB-231 cells (which express a functionally compromised mutant p53) (fig. S1A).

MCF-$7^{GLU}$ cells exhibited high rates of glucose-dependent extracellular acidification (ECAR) (Fig. 1B). In contrast, in MCF-$7^{FRU}$ cells, fructose resulted in barely detectable ECAR that could not even be increased when oligomycin was used to inhibit mitochondrial respiration (Fig. 1B). Furthermore, addition of glucose to temporarily glucose-starved MCF-$7^{GLU}$ cells decreased oxygen consumption (The Crabtree effect), whereas fructose did not similarly affect MCF-$7^{FRU}$ cells (fig. S1B). Thus, compared to MCF-$7^{GLU}$ cells, rates of fructose import into MCF-$7^{FRU}$ cells enabled very low levels of flux through the ATP- and NADH-generating stages of glycolysis and little conversion of pyruvate to lactate. In comparison, ZR-75-$1^{GLU}$ cells were less glycolytic than MCF-$7^{GLU}$ cells, and consequently, although ECAR was further decreased in ZR-75-$1^{FRU}$ cells,

the effect was much less pronounced than that in MCF-7 cells (fig. S1B). As further confirmation of decreased glycolytic flux in the fructose-cultured cells, a fluorescent biosensor of the NADH:$NAD^+$ ratio (Peredox, fig. S1C) (*11*) was expressed in MCF-7 cells and revealed a statistically significant decrease in NADH abundance after adaptation to culture in fructose (Fig. 1C).

Similarly to many nontransformed and cancer cells that retain expression of wild-type p53, MCF-$7^{GLU}$ cells had readily detectable p53 protein (Fig. 1D, left). We found that p53 was not homogeneously distributed, but rather was present at high amounts in the nuclei of approximately 10 to 20% of the cells (Fig. 1D, middle). This is likely due to short pulses of p53 accumulation during cell cycle progression (*49*). In contrast, MCF-$7^{FRU}$ cells demonstrated a reduction in total p53 abundance to 39 ± 3% of that in MCF-$7^{GLU}$ cells (Fig. 1D, left), as well as a loss of the high p53-expressing cells (Fig. 1D, middle). Induction of p53 by the DNA damaging agent doxorubicin was not suppressed in MCF-$7^{FRU}$ (cells fig. S1D). Culture of MCF-$7^{GLU}$ cells in medium lacking sugar resulted in p53 accumulation (fig. S1E), as was previously reported (*28*). Because MCF-$7^{FRU}$ cells proliferate at least as fast as MCF-$7^{GLU}$ cells, the pulses of p53 accumulation in proliferating cells may be dependent upon the cycling cells having a glycolytic phenotype. In the less glycolytic ZR-75-1 cells, the change in carbohydrate source had a lesser effect on p53 abundance (Fig. 1D, right).

A detectable proportion of the p53 protein present in MCF-7$^{GLU}$ cells, but not MCF-7$^{FRU}$ cells, was phosphorylated at Ser$^{15}$ (Fig. 1D, left). Therefore, the p53 in MCF-7$^{GLU}$ cells may be active as a positive regulator of gene transcription. To determine whether this was the case, we examined the expression of a panel of known p53-responsive genes in the cells (Fig. 2A, left). When mRNA abundance in glycolytic MCF-7$^{GLU}$ cells was plotted relative to their abundance in non-glycolytic MCF-7$^{FRU}$ cells, a positive effect of glycolysis on the expression of multiple p53-responsive genes was revealed. Furthermore, in the mutant p53-expressing MDA-MB-231 cell line, the abundance of most of these mRNAs was insensitive to glycolysis. In the wild type p53-expressing ZR-75-1 cells, a positive effect of glycolysis on the abundance of p53-responsive mRNAs was also observed (Fig. 2A, right), although the magnitude of the effect was lower than that in MCF-7 cells. This is consistent with the lower rates of glycolysis in ZR-75-1 cells and the smaller effect on p53 protein abundance; however, it does confirm that the effects of glycolysis on p53-dependent transcriptional programs occurs in a cell line other than MCF-7 cells. To determine the p53-dependency of the expression of these genes in MCF-7$^{GLU}$ cells, p53 was either knocked down with siRNA (Fig. 2B, left; see fig. S2 for knockdown experiments) or further induced with the HDM2 inhibitor, nutlin-3 (Fig. 2B, right). This experiment confirmed that the expression of most of the transcripts (for example, *DDB2*, *HDM-P2*, and *CDKN1A*) was indeed p53-dependent, but for some genes (for example, *DRAM1*) the regulation appeared to be more complex.

Because the expression of p53 was restricted to a small subset of cells in the MCF-7$^{GLU}$ cultures, we then performed whole-transcriptome, single-cell mRNA-sequencing to examine the effects of restricted glycolysis on the p53-dependent transcriptional response in single cells. Using data from

344 MCF-$7^{GLU}$ and 416 MCF-$7^{FRU}$ cells, we first generated a glycolysis gene expression score for each cell based on a 29-gene set (see Supplementary Materials), and used this to identify cells with the highest glycolysis scores, and which were thus likely to have the highest potential for the induction of glycolytic stress. We found that there was an approximately 9-fold increase in the number of cells with the highest scores (>0.35 cuff-off) in MCF-$7^{GLU}$ cells compared to that in MCF-$7^{FRU}$ cells (Fig. 2C, left) Conversely, in MCF-$7^{FRU}$ cells, the percentage of transcripts originating from mitochondrial DNA was relatively increased (Fig. 2C, middle), indicating a compensatory increase in mitochondrial biogenesis in those cells in which glycolysis was restricted. We then used a validated set of 116 p53-activated target genes (*50*) to generate a p53-activity score for each cell. Application of a cut-off threshold to identify cells with a high p53-activity score (>0.1) identified 6.7% of MCF-$7^{GLU}$ cells and 2.2% of MCF-$7^{FRU}$ cells (Fig. 2C, right). These data are thus consistent with the global transcriptional changes in p53 response-genes that we identified (Fig. 2) being focused in a subset of cells that are more prevalent in MCF-$7^{GLU}$ cells than in MCF-$7^{FRU}$ cells. This finding is also consistent with the heterogeneity of protein abundance that we identified earlier (Fig. 1D).

We then proceeded to further examine the nature of the cells with a high p53 activity score in the MCF-$7^{GLU}$ cells only. Differential gene expression analysis between the cells with a high p53 activity score (>0.1) and those with a low score (≤0) identified the gene with the highest relative expression in the high p53 activity score cells to be *CDKN1A*, and in the low scoring group to be the proliferation marker *MKI67* (fig. S3A). Consistent with this, application of a cell cycle phase score to the cells demonstrated that most of the cells with high p53 activity were in G1 phase (Fig.

2D, left). In contrast, the cells with high glycolysis scores were concentrated in the S and G2M phases (Fig. 2D, right) and relatively few had a high p53 activity score (fig. S3B). Given that pulses of increased p53 protein abundance in proliferating cells are known to only last approximately 3 hours (*49*), and that these pulses by definition precede expression of the p53 target genes (*51*), a lack of overlap between the p53-activating signal and the peak expression of p53-target genes is to be anticipated. The data are consistent with a small fraction of highly glycolytic cells inducing a p53 response, potentially in S phase where cellular NADH:$NAD^+$ ratios are greatest (*52*), followed by subsequent *CDKN1A*-induced protective G1 arrest, although the precise pattern of p53 induction is likely to be confounded by the effects of other transient stresses, such as DNA damage (*49*). Note that with respect to the potential effects of p53 on metabolism, those cells with the greatest p53 activity were characterized by the expression of *GDF15* and *TP53INP1*, both p53-responsive genes whose products mediate protection from ROS (*53, 54*). Furthermore, examination of the expression of genes encoding specific glycolytic enzymes in this dataset (fig. S3, C and D) showed that those involved in the latter stages of glycolysis were most consistently decreased in expression in the cells with high p53 activity, with TPI1 showing the most statistically significant differential. This also is consistent with these cells diverting glucose carbon into the pentose phosphate pathway to provide reducing equivalents for protection from ROS (*55*), in line with previously understood p53-induced protective responses (*25*).

**Inhibiting LDH increases p53 abundance and activity**

To investigate the nature of the pathway that signals from glycolysis to p53, we wished to suppress glycolysis at a different point in the pathway to induce a differential effect on glycolytic intermediates to those caused by culture in fructose. We therefore inhibited the LDH-dependent regeneration of $NAD^+$ from NADH. Using the Peredox biosensor, we first confirmed that suppression of cellular LDH activity resulted in the expected inhibition of $NAD^+$ regeneration from NADH in MCF-$7^{GLU}$ cells. LDH is a tetrameric enzyme consisting of *LDHA* and *LDHB*-encoded subunits, with LDHA being the predominant form in highly glycolytic cells (*17*). LDHA-specific siRNA statistically significantly increased the NADH:$NAD^+$ ratio (Fig. 3A, left). We found that p53-specific siRNA had a comparable effect (Fig. 3A, left), consistent with a role for p53 in the suppression of glycolysis and promotion of OXPHOS. The LDH inhibitor, sodium oxamate (50 mM) also increased the NADH:$NAD^+$ ratio in MCF-7 cells (Fig. 3A, right). We then titrated sodium oxamate in MCF-$7^{GLU}$ cells to determine the optimal concentration for the inhibition of aerobic glycolysis (Fig. 3B). Glucose-dependent ECAR was suppressed by concentrations of oxamate between 10 and 50 mM. At 50 mM and greater concentrations, oxamate also modestly suppressed oxygen consumption, indicating that it had effects on targets other than LDH at these concentrations. A 2-hour incubation of MCF-$7^{GLU}$ cells with 25 mM oxamate did not reduce ATP abundance, and an apparent modest reduction at 50 mM was not statistically significant (Fig. 3C). The concentration range of oxamate at which ECAR was inhibited also overlapped with the dose required to inhibit MCF-$7^{GLU}$ cell proliferation (Fig. 3D) and colony forming ability (Fig. 3D). Compared to MCF-$7^{GLU}$ cells, MDA-MB-$231^{GLU}$ cells required higher concentrations of oxamate to inhibit their colony-forming ability (Fig. 3E). LDHA-specific siRNA also decreased MCF-$7^{GLU}$ cell proliferation (Fig. 3D). After a time course analysis of the effects of 50 mM oxamate on p53 protein abundance in MCF-$7^{GLU}$ cells (Fig. 3F, left), we performed an

oxamate dose-response analysis with a 2-hour exposure that demonstrated that concentrations of 25 mM and greater induced a rapid accumulation of p53 protein (Fig. 3F, middle), with expression after exposure to 50 mM oxamate increasing to 218 ± 1% of untreated controls (Fig. 3F, right). The p53-inducible protein HDM2 was also increased by 50 mM oxamate (Fig. 3F, left). LDHA-specific siRNA also induced the accumulation of p53 protein (Fig. 3F, middle), as did 50 mM lactate (Fig. 3G). Both treatment with LDHA-specific siRNA (for 72 hours) (Fig. 3H) and 25 to 50 mM oxamate (for 6 hours) (Fig. 3I) induced the expression of multiple p53-responsive gene transcripts, including *CDKN1A* and *PUMA*. The relative magnitude of induction of the individual p53-responsive genes differed between these two approaches, which may be due to differences either in the mechanisms of action of the siRNA and the small-molecule inhibitor or the kinetics of LDH inhibition and transcriptional response studied. also examined the effect of lactate on p53-dependent gene expression (fig. S4). We also confirmed that the oxamate-induced, p53-dependent transcriptional response did not involve AMP-AMPK signaling (fig. S5).

Therefore, these two distinct methods of inhibiting glycolysis had opposing consequences for the activation of p53 in the cell. When glucose import was low such that there were low rates of flux through phospho-fructokinase into the latter stages of glycolysis, p53 abundance was decreased. However, when the block was at a later stage in the pathway, such that the accumulation of metabolites in the later stages of glycolysis was induced, p53 abundance increased. As we have shown, NADH was oppositely affected by the two treatments, consistent with a potential role in the signal to p53. We therefore proceeded to examine whether an NADH-CtBP signaling pathway could be controlling p53 in response to changes in glycolytic metabolism.

**A role of the CtBP family of NADH-regulated transcriptional regulators in the regulation of p53 abundance by glycolysis**

We have previously established a method of cell synchronization, followed by transfection with CtBP-specific siRNA at the time of release, to determine the effects of CtBP suppression on specific stages of the cell cycle (*56*). We used this model to establish whether loss of CtBPs might influence p53 activity, independently of their effects on mitotic fidelity that we have previously described. As shown by both Western blotting (Fig. 4A) and single-cell immunofluorescence (Fig. 4B), when compared to control siRNA–transfected MCF-7$^{GLU}$ cells, cells in which the expression of CtBP1 and CtBP2 was knocked down by siRNA showed a marked increase in p53 protein abundance by 24 hours after release from G1 arrest. Comparison with the cell cycle analysis (Fig. 4A) demonstrated that CtBPs were required for the prevention of spontaneous accumulation of p53 in S phase. p53 also accumulated in response to CtBP knockdown in MCF-7$^{FRU}$ cells (Fig. 4C), which is consistent with a model in which CtBPs promote p53 turnover in nonglycolytic cells.

To investigate which activities of CtBPs were responsible for their p53-suppressing activity, we used our approach of microinjection of dominant-negative fragments of CtBPs to dissect CtBP function (*56*). Microinjection of MCF-7$^{GLU}$ cells with an N-terminal fragment of CtBP2 (CtBP$^{DN}$) designed to be targeted to the cell nucleus and disrupt the interaction of CtBPs with multiple protein partners including HDM2, resulted in the accumulation of p53 protein in most of the

injected nuclei (Fig. 4D and fig. S6A). Comparable results were obtained by transfection of MCF-7 cells with a plasmid encoding an EGFP-CtBP$^{DN}$ fusion protein (fig. S6B). In contrast, a mutated form of this construct (CtBP$^{DN\Delta NLS}$) lacking the N-terminal domain amino acids that constitute both a nuclear localization sequence and an HDM2-binding region, failed to induce p53 when microinjected (Fig. 4D). In a previous analysis (*56*), we further dissected the contribution of the two functions of this region by microinjection directly into the nucleus; however, this was not possible here, because nuclear microinjection alone induced p53 accumulation. A single point mutation (V72R) in the PxDLSx-binding domain with which it interacts with most of its protein partners also rendered CtBP$^{DN}$ unable to induce p53 accumulation, suggesting that complexes involving PxDLS motif–containing proteins are important in the CtBP-dependent regulation of p53 abundance (Fig. 4D). We then compared the effects of CtBP$^{DN}$ with those of CtBP$^{DD}$, which contains the central dimerization domain of CtBP2, and is designed to inhibit CtBP dimerization. Whereas we previously showed that CtBP$^{DD}$ disrupts the fidelity of mitosis (*47*), it does not induce p53 protein accumulation. Consistent with this latter finding, our previously described, cell-permeable cyclic peptide inhibitor of CtBP dimerization, CP61-TAT (*47*), also did not induce p53 protein accumulation (Fig. 4E). Together, these data suggest that monomeric forms of CtBP, in complex with other protein partners including, potentially, HDM2, are required for the suppression of p53 protein accumulation. Given that binding to NADH drives CtBPs into the dimeric form, we hypothesized that the accumulation of p53 in highly glycolytic cells or in cells in which NADH accumulates due to LDH inhibition was driven by the NADH-dependent loss of CtBP monomers. This conclusion is consistent with our earlier studies of the effects of overexpressed full-length CtBP2 proteins on p53-dependent transcription (*43*).

**Evidence for an NADH-CtBP-p53 pathway that regulates cell proliferation and survival in response to glycolytic stress**

We next determined whether the p53 protein that accumulated in response to the loss of CtBPs was active. siRNA-mediated CtBP depletion from MCF-7$^{GLU}$ cells resulted in the induction of most of the p53-response genes tested (Fig. 5A). Overall, the magnitude of the effect was greater than that obtained by changing the carbohydrate source or suppressing LDH, but less than the response to nutlin-3. The relative magnitude of response for different genes also differed between the different interventions. For example, *CDKN1A* was one of the lesser induced genes in response to CtBP1/2 knockdown, whereas it was consistently one of the more robustly induced genes in response to the other interventions. Note that several genes involved in the regulation of cellular redox and metabolic pathways (*TP53INP1*, *SESN1*, *TIGAR*) were induced by CtBP loss. To determine the potential effect of CtBPs on cellular metabolism, we used the Seahorse instrument to study MCF-7$^{GLU}$ cells after knockdown of p53 and of CtBPs. Knockdown of CtBPs alone caused reductions in both ECAR and OCR in glucose-cultured cells, whereas p53-specific siRNA caused only a small decrease in OCR (Fig. 5B, left and middle). A more substantial effect on OCR was caused by the combination of CtBP and p53 knockdown. This was not merely indicative of a reduced demand for ATP, because the oxidative capacity of the cells (as revealed by uncoupling mitochondrial respiration from ATP demand with FCCP) was markedly reduced relative to the glycolytic capacity (as revealed by inhibiting mitochondrial ATP synthesis with oligomycin, hence releasing glycolytic enzymes from ATP-mediated negative feedback) (Fig. 5B, middle and right). These two capacities are primarily determined by the expression of genes involved in the metabolic pathways, and p53-dependent stress responses control gene expression to suppresses glycolysis and promote oxidative phosphorylation (*24, 26, 57*). Therefore, the fact that this ratio was only

disrupted when both CtBPs and p53 were knocked down simultaneously can be explained if there exists an auto-compensatory relationship between CtBPs and p53, which regulates metabolic homeostasis through the control of gene expression. To further investigate the role of the NADH-binding by CtBPs on their regulation of glycolysis, we stably over-expressed in MCF-7$^{GLU}$ cells either wild-type CtBP2 or an NADH-binding–incompetent CtBP2 mutant (G189A) (Fig. 5C, left). Compared to the parental line, a panel of control transfected clones and the wild-type CtBP2-expressing clone, CtBP2$^{G189A}$ cells exhibited an increase in basal glycolysis compared to that in the other lines (Fig. 5C, right). This finding lends further support to a model in which the loss of NADH-free forms of CtBPs in glycolytic cells acts as a negative feedback signal to maintain glycolytic homeostasis.

To determine the potential implications of this pathway for cancer cell survival in response to altered cellular metabolism, we examined the colony-forming capacity of MCF-7$^{GLU}$ cells after knockdown of CtBPs, p53, or LDHA alone or in combination (Fig. 5D). CtBP1/2-specific siRNA resulted in statistically significantly decreased colony numbers, and, consistent with our previous work (*44*), cell survival was further decreased when p53 was also knocked down. Thus, the induction of p53 in response to CtBP loss is pro-survival. In contrast, whereas knockdown of LDHA resulted in decreased colony numbers, this effect was reversed when p53 was also knocked down. This implies that the effects of LDHA-specific siRNA on colony formation were either due to the suppression of glycolysis, and that p53-specific siRNA overcame this by increasing glycolysis, or they were due to the induction of a p53-dependent, anti-proliferative response. In either case, it appears that, in the absence of p53, cells show a higher propensity to maintain

proliferation under conditions where their rates of glycolysis would otherwise exceed the capacity of LDH to regenerate $NAD^+$.

**Mechanisms of regulation of p53 by CtBP proteins**

CtBP2 has an HDM2-binding site in its N-terminal domain, preferentially binds to HDM2 in its NADH-free form, and inhibition of p53-dependent transcription by CtBPs can be HDM2-dependent (*43, 56*). Because we had established that CtBPs had a potentially direct effect on p53 protein abundance, we investigated their effect on p53 ubiquitylation, which is driven by HDM2. When MCF-$7^{GLU}$ cells in early S phase were analyzed by Western blotting to detect p53, overexposure of the Western blots showed a ladder of high molecular weight bands (Fig. 6A), which are consistent with ubiquitylated p53 (*58*). Band intensity increased when the proteasome-mediated degradation of ubiquitylated p53 was blocked by MG132. In contrast, in cells transfected with CtBP1/2-specific siRNA, these high molecular weight p53 bands were less readily detectable, and did not substantially increase with MG132 treatment. Therefore we conclude that, in normally proliferating cells, ongoing ubiquitylation of p53 was at least partially dependent upon CtBPs. In addition, CtBPs bound to both p53 and HDM2 in these cells (Fig. 6B).

Blockade of HDM2-mediated p53 degradation can occur through multiple mechanisms depending on the stress involved. These include classic pathways such as those induced by ATP depletion

and genotoxic stress being posttranslational modifications (PTMs) at the N- and C-termini of p53 that interfere with HDM2-binding and ubiquitylation, whereas other pathways, such as those induced by ribosomal stress, involve primary effects on protein-protein interactions. To investigate the mechanism whereby CtBP loss promoted p53 accumulation and activity, we examined the role of PTMs. We performed a time-course analysis of the accumulation of multiple p53 PTMs in response to CtBP knockdown in MCF-7$^{GLU}$ cells (Fig. 6C and fig. S7). We found that, compared to that in control siRNA–treated cells, p53 protein abundance began to increase within 24 hours of the release of CtBP-depleted cells from serum starvation. Phosphorylation at the major N-terminal PTM site, Ser$^{15}$, also increased, though this was not readily apparent until the 48-hour time point. The pSer$^{37}$ signal in these cells was weak relative to those in the nutlin-3– or doxorubicin-treated controls. The abundance of p53-pSer$^{392}$ increased approximately in line with p53 accumulation, and there was a modest increase in the appearance of p53 acetylated at Ser$^{382}$ by 48 hours (Fig. 6C). To determine whether phosphorylation at Ser$^{15}$ was required for p53 accumulation, we added inhibitors of signaling protein kinases to the cells (Fig. 6D). The ATM inhibitor KU55933 partly suppressed the phosphorylation of p53 at Ser$^{15}$ in cells treated with CtBP1/2-specific siRNA (Fig. 6D). However, whereas KU55933 blocked p53 protein accumulation in response to neocarzinostatin, p53 protein still accumulated in CtBP-depleted cells in which ATM-dependent phosphorylation of Ser$^{15}$ was blocked. A lack of dependency on ATM-signaling for CtBP knockdown–induced p53 protein activity was confirmed by analysis of the induction of p53 target genes (Fig. 6E). Regulation of p53 by CtBPs may therefore involve protein-protein interactions, rather than classical PTM pathways, with the late induction of PTMs that we observed (Fig. 6C) being potentially due to the previously reported effects of CtBP depletion on mitotic fidelity (*44*).

## DISCUSSION

The initial paradigm of p53 function as "guardian of the genome" (*59*) proposed that the function of p53 that was inhibited by p53-binding oncoproteins such as HDM2 was its ability to protect cells from the mutagenic consequences of genotoxic stress. p53 is now known to respond to, and regulate, many other pathways. Of these, p53-regulated gene expression networks that control cell metabolism have perhaps some of the most fundamental implications in health and disease (*22*, *24*). p53 limits flux though the latter stages of glycolysis before GAPDH-dependent $NAD^+$ reduction, while promoting ATP generation by OXPHOS and protection from ROS by promoting flux through the pentose phosphate pathway. Furthermore, its induction of genes such as *CDKN1A* decreases metabolic demand by inducing cell cycle arrest. Consequently, p53 protects cells from metabolic stresses such as glucose starvation–mediated ATP depletion (*28*) and serine starvation (*29*). Our delineation of a protective p53 response in cells that are driven to undergo high rates of glycolytic metabolism that exceed their ability to maintain it through LDH-dependent $NAD^+$ regeneration adds to our understanding of the role of p53 metabolic homeostasis (Fig. 7).

Our mechanistic analysis of this pathway builds upon our earlier work that showed that CtBPs bind to HDM2 in an NADH-dependent manner to suppress p53-dependent transcription from specific target promoters, and that CtBP depletion by siRNA induces a p53 response that protects against the loss of mitotic fidelity that is also induced by CtBP loss (*43, 44, 56*). Here, our kinetic

analysis demonstrates that the induction of p53 accumulation upon CtBP loss occurs before this effect on mitosis. It also precedes, and is independent of, the DNA-damage induced ATM-p53-pSer$^{15}$ signaling cascade. Overall, our data support a model whereby CtBPs are required for effective HDM2-dependent ubiquitylation and degradation of p53 in proliferating cells. Their loss results in the accumulation of p53 in sufficient amounts to induce a robust transcriptional response. Because the NADH-free, monomeric forms of CtBPs that interact with HDM2, the increase in NADH abundance under glycolytic stress results in a loss of CtBP-regulated HDM2 activity, and thus increased p53 accumulation.

*TP53* is one of the most frequently mutated genes in human cancer (*60*). Given that, in most cell types in the absence of stress, p53 is rendered essentially nonfunctional through rapid rates of proteasome-mediated degradation, the presence of stress-signals that activate p53 must be a near-ubiquitous occurrence in human cancer, otherwise p53-inactivating mutations would not be selected for (*61*). However, whereas there are exceptions, such as where DNA-damaging chemotherapy appears to select for tumor cells with treatment-induced p53 mutations (*62*), in most chemo-naïve tumors, the nature of the p53-activating stress is harder to define. Increased rates of aerobic glycolysis are also an extremely common event during many cancers, and they tend to increase further with cancer progression (*2, 10*). Furthermore, as tumors expand in the absence of a well-developed blood supply, the tumor micro-environment becomes acidified, through the build-up of glycolytic lactate (*13*), which, combined with an increase in glycolysis, drives an increase in the intracellular NADH:$NAD^+$ ratio by inhibiting LDH (*63*). Here, we showed that this inherent hallmark of most cancer cells acts as a p53-activating stress. This p53-dependent

glycolytic stress response pathway could potentially serve as a selection pressure for the acquisition of p53 mutations in a high percentage of human tumors. p53 mutation-containing cells in these hostile micro-environments would continue to proliferate at rates that exceed the ability of glycolysis to provide metabolites for pathways such as nucleotide biosynthesis or ROS protection. Whereas cell death may initially increase in these cells due to increased cellular damage, the increased DNA mutation rates would further promote tumor progression in the cells that do survive (Fig. 7). Our findings are entirely consistent with the observations of Chen *et al.* (*30*), who identified a lactic acidosis–induced gene expression signature in normal mammary epithelial cells, and then, in a cohort of breast cancer patients, showed that this signature is associated with both a wild-type p53 gene status and good prognosis.

## MATERIALS AND METHODS

### Cell culture, cell cycle analysis, and reagents

Cell culture and analysis of cell DNA content was performed as previously described (*44*). Cells used were (MCF-7[ATCC® HTB-22™], ZR-75-1 [ATCC® CRL-1500™] and MDA-MB-231 [ATCC® HTB-26™]). For media with different sugars, 25 mM glucose or 10 mM fructose was added to glucose-free DMEM (Sigma #D5030) supplemented with 3.7 g/L sodium bicarbonate, 2 mM glutamine, 1 mM sodium pyruvate and 10% fetal bovine serum. Cells were grown for ≥ 21 days with fresh medium added every 2 to 3 days. KU55933, SB202190, and wortmannin were

obtained from Tocris,. Sodium oxamate, MG132, and neocarzinostatin was obtained from Sigma. Nutlin-3 was obtained from Enzo life sciences.

**Western blotting, immunofluorescence, and RNAi**

Western blotting and immunofluorescence analyses and RNAi-based experiments were performed as described previously (*44*). The following antibodies were used: CtBP1 (E12; Santa Cruz Biotechnologies), CtBP2 (clone 16; BD biosciences), LDHA (C4B5; Cell Signaling Technology), p53 (DO-1; AbD Serotec), pSer15-p53, pSer37-p53, pSer392-p53 and ac382-p53 (Cell Signaling Technology), HDM2 (2A10; Abcam), and GFP (Abcam). siRNA reagents targeting CTBP1/2 and TP53 were previously described (*44*). LDHA-specific siRNA (#s229664) was obtained from Life Technologies. CP61-TAT and TAT were synthesized as described previously (*47*).

**Seahorse assays**

ECARs and OCRs were calculated using a Seahorse XF96 (Agilent) with the glycolytic stress test or mitochondrial stress test according to the manufacturer's guidelines. Cells were plated at a density of 18,000/well 18 hours before the assay. Data were normalized to total protein per well. Glycolytic capacity = ([ECAR after oligomycin] – [ECAR after 2-deoxyglucose]); mitochondrial respiratory capacity = ([OCR after FCCP] – [OCR after rotenone + antimycin]).

**Cell proliferation, ATP analysis, and colony forming assays**

Cell proliferation was assessed using the xCELLigence real-time analysis system (ACEA Biosciences). Cells were plated at 5000/well and proliferation was followed for 100 hours. For ATP analysis, 5000 cells/well were plated in 96-well plates. Twenty-four hours later, metabolic inhibitors were added to the medium. After 2 hours of incubation, ATP was analyzed with an ATPlite Luminescence ATP Detection Assay System (Perkin Elmer), according to the manufacturer's instructions. Assay medium was transferred to white-welled plates and analyzed with a Varioskan Flash instrument (Thermo Scientific). After background subtraction, the means of technical replicates for each independent experiment were first calculated, and then the data were presented as means ± SEM for three independent experiments. Colony-forming assays were performed by plating single cells at low density for 10 days before colonies were counted. Where the effects of siRNA-mediated knockdown on colony-forming is shown, the mean of triplicate cell plates was first calculated and then the data were presented as means ± SEM from independent experiments.

**Transfection, overexpression, and microinjection**

The CtBP2 and CtBP2$^{G189A}$ constructs for overexpression analysis and the CtBP2-GFP construct for immunoprecipitation were generated as described previously (*43*) and were used in the

transfection of cells with FugeneHD (Promega). Immunoprecipitation was performed with GFP-Trap A (Chromotek). The pcDNA3.1-Peredox-mCherry-NLS plasmid was a gift from Gary Yellen (Addgene plasmid #32384) and used to transfect cells at 2 µg DNA/well with FugeneHD (Promega). Seventy-two hours after transfection, the cells were transferred to assay medium [serum- and sodium bicarbonate–free DMEM (Sigma #D5030), 2 mM Hepes (pH 7.4), 25 mM glucose, 1 mM sodium pyruvate, 2 mM glutamine] before imaging. Fluorescence images were captured with an Olympus IX81 microscope. Fluorescence quantification from captured images was performed with ImageJ software. The changes in fluorescence in response to the NADH:$NAD^+$ ratio were calculated as described by Hung *et al.* (*11*). GST and GST-fusion proteins were expressed, purified, and microinjected as described previously (*43, 56*).

**RNA analysis**

Total RNA was isolated from cells with the RNA ReliaPrep system (Promega) and treated with DNase1. RNA was reverse-transcribed with M-MLV reverse transcriptase and oligo(dT) primer (Promega). Quantitative PCR analysis was performed with a 7500 Real-Time PCR system (Applied Biosystems); for information on the primers used, see table S1. Relative RNA abundance was calculated by the $\Delta\Delta C_T$ method using *ACTB* (Applied Biosystems #4326315E) as endogenous control. The mean of technical qPCR duplicates was first calculated for each sample, and then data are presented as means ± SEM from independent experiments. One-sample *t* tests on the mean response of each gene in the panel were used to determine the statistical significance of the p53-induced gene expression signature (outliers were discarded using Grubb's test).

**Whole-transcriptome, single-cell mRNA sequencing (Drop-seq)**

Using a custom microfluidic workstation (https://dropletkitchen.github.io/), experiments were performed according to the microfluidic device design and protocol of Macosko *et al.* (*64*) with the following adjustments: 13 PCR cycles and 500 pg cDNA from a total of 1000 cells per culture condition, combined from three independent experiments, was used as a template for Nextera XT library preparation. Libraries were sequenced on the Illumina NextSeq 500 platform. Raw sequencing reads were aligned to hg19 and binned/collapsed onto the cell barcodes corresponding to individual mRNA capture beads using Drop-seq tools (*64*) (http://mccarrolllab.com/dropseq). To exclude low-quality cells and likely cell doublets, cells with fewer than 2000 genes and greater than 15,000 unique molecular identifiers (UMIs) were removed. All genes that were not detected in at least three cells were discarded, and all mitochondrial DNA-encoded genes were excluded, leaving 15,946 genes across 760 cells (344 MCF-$7^{GLU}$ cells and 416 MCF-$7^{FRU}$ cells). The digital gene expression matrix was library-size normalized, scaled by the total number of transcripts, multiplied by 10,000, and natural-log transformed before further downstream analysis with Seurat (http://satijalab.org/seurat/) (*64*). R Scripts are provided in Supplementary Methods.

**Statistical analysis**

GraphPad Prism software (GraphPad) was used for statistical analysis. When *t* tests were used, they were two-sided. For all statistical analysis: $*P < 0.05$, $**P < 0.01$, $***P < 0.001$.

**SUPPLEMENTARY MATERIALS**

Fig. S1. Effects of altered media sugar composition on proliferation, metabolism, and p53 abundance in breast cancer cells.

Fig. S2. Validation of siRNA efficacy in MCF-7 cells.
Fig. S3. Extended analysis of single-cell mRNA sequencing of MCF-7 cells.
Fig. S4. The effect of lactate on the induction of p53-responsive genes.
Fig. S5. The effect of AMPKα-specific siRNA on the induction of p53-responsive genes by oxamate.
Fig. S6. Effect of dominant-negative CtBP fragments on p53 abundance in MCF-7 cells.
Fig. S7. Quantification of the effect of CtBP1/2-specific siRNA on p53 posttranslational modifications.
Table S1. The qPCR primers and probes used in this study.
Glycolysis Gene Annotation list for Dropseq analysis
R Script for Dropseq analysis

**REFERENCES AND NOTES**


1. O. Warburg, On the origin of cancer cells. *Science* **123**, 309-314 (1956).

2. A. Schulze, A. L. Harris, How cancer metabolism is tuned for proliferation and vulnerable to disruption. *Nature* **491**, 364-373 (2012).

3. E. Mullarky, L. C. Cantley, in *Innovative Medicine: Basic Research and Development*, K. Nakao, N. Minato, S. Uemoto, Eds. (Tokyo, 2015), pp. 3-23.

4. N. N. Pavlova, C. B. Thompson, The Emerging Hallmarks of Cancer Metabolism. *Cell Metab* **23**, 27-47 (2016).

5. A. L. Lehninger, D. L. Nelson, M. M. Cox, *Principles of Biochemistry*. (Worth, New York, ed. 2, 1992).

6. A. P. Halestrap, Monocarboxylic acid transport. *Comprehensive Physiology* **3**, 1611-1643 (2013).

7. Q. Zhang, D. W. Piston, R. H. Goodman, Regulation of corepressor function by nuclear NADH. *Science* **295**, 1895-1897 (2002).

8. J. H. Ostrander, C. M. McMahon, S. Lem, S. R. Millon, J. Q. Brown, V. L. Seewaldt, N. Ramanujam, Optical redox ratio differentiates breast cancer cell lines based on estrogen receptor status. *Cancer Res* **70**, 4759-4766 (2010).

9. M. G. Vander Heiden, L. C. Cantley, C. B. Thompson, Understanding the Warburg effect: the metabolic requirements of cell proliferation. *Science* **324**, 1029-1033 (2009).

10. R. J. DeBerardinis, J. J. Lum, G. Hatzivassiliou, C. B. Thompson, The biology of cancer: metabolic reprogramming fuels cell growth and proliferation. *Cell Metab* **7**, 11-20 (2008).

11. Y. P. Hung, J. G. Albeck, M. Tantama, G. Yellen, Imaging cytosolic NADH-NAD(+) redox state with a genetically encoded fluorescent biosensor. *Cell Metab* **14**, 545-554 (2011).

12. S. Walenta, W. F. Mueller-Klieser, Lactate: mirror and motor of tumor malignancy. *Semin Radiat Oncol* **14**, 267-274 (2004).

13. R. A. Gatenby, R. J. Gillies, Why do cancers have high aerobic glycolysis? *Nat Rev Cancer* **4**, 891-899 (2004).

14. J. W. Locasale, A. R. Grassian, T. Melman, C. A. Lyssiotis, K. R. Mattaini, A. J. Bass, G. Heffron, C. M. Metallo, T. Muranen, H. Sharfi, A. T. Sasaki, D. Anastasiou, E. Mullarky, N. I. Vokes, M. Sasaki, R. Beroukhim, G. Stephanopoulos, A. H. Ligon, M. Meyerson, A. L. Richardson, L. Chin, G. Wagner, J. M. Asara, J. S. Brugge, L. C. Cantley, M. G. Vander Heiden, Phosphoglycerate dehydrogenase diverts glycolytic flux and contributes to oncogenesis. *Nat Genet* **43**, 869-874 (2011).

15. R. Possemato, K. M. Marks, Y. D. Shaul, M. E. Pacold, D. Kim, K. Birsoy, S. Sethumadhavan, H. K. Woo, H. G. Jang, A. K. Jha, W. W. Chen, F. G. Barrett, N. Stransky, Z. Y. Tsun, G. S. Cowley, J. Barretina, N. Y. Kalaany, P. P. Hsu, K. Ottina, A. M. Chan, B. Yuan, L. A. Garraway, D. E. Root, M. Mino-Kenudson, E. F. Brachtel, E. M. Driggers, D. M. Sabatini, Functional genomics reveal that the serine synthesis pathway is essential in breast cancer. *Nature* **476**, 346-U119 (2011).

16. A. Le, C. R. Cooper, A. M. Gouw, R. Dinavahi, A. Maitra, L. M. Deck, R. E. Royer, D. L. Vander Jagt, G. L. Semenza, C. V. Dang, Inhibition of lactate dehydrogenase A induces oxidative stress and inhibits tumor progression. *Proc Natl Acad Sci U S A* **107**, 2037-2042 (2010).

17. V. R. Fantin, J. St-Pierre, P. Leder, Attenuation of LDH-A expression uncovers a link between glycolysis, mitochondrial physiology, and tumor maintenance. *Cancer Cell* **9**, 425-434 (2006).

18. J. R. Doherty, J. L. Cleveland, Targeting lactate metabolism for cancer therapeutics. *J Clin Invest* **123**, 3685-3692 (2013).

19. P. E. Porporato, S. Dhup, R. K. Dadhich, T. Copetti, P. Sonveaux, Anticancer targets in the glycolytic metabolism of tumors: a comprehensive review. *Frontiers in pharmacology* **2**, 49 (2011).

20. M. E. Pacold, K. R. Brimacombe, S. H. Chan, J. M. Rohde, C. A. Lewis, L. J. Swier, R. Possemato, W. W. Chen, L. B. Sullivan, B. P. Fiske, S. Cho, E. Freinkman, K. Birsoy, M. Abu-Remaileh, Y. D. Shaul, C. M. Liu, M. Zhou, M. J. Koh, H. Chung, S. M. Davidson, A. Luengo, A. Q. Wang, X. Xu, A. Yasgar, L. Liu, G. Rai, K. D. Westover, M. G. Vander Heiden, M. Shen, N. S. Gray, M. B. Boxer, D. M. Sabatini, A PHGDH inhibitor reveals coordination of serine synthesis and one-carbon unit fate. *Nat Chem Biol* **12**, 452-458 (2016).

21. M. A. Reid, A. E. Allen, S. Liu, M. V. Liberti, P. Liu, X. Liu, Z. Dai, X. Gao, Q. Wang, Y. Liu, L. Lai, J. W. Locasale, Serine synthesis through PHGDH coordinates nucleotide levels by maintaining central carbon metabolism. *Nature communications* **9**, 5442 (2018).

22. F. Kruiswijk, C. F. Labuschagne, K. H. Vousden, p53 in survival, death and metabolic health: a lifeguard with a licence to kill. *Nat Rev Mol Cell Biol* **16**, 393-405 (2015).

23. H. F. Horn, K. H. Vousden, Coping with stress: multiple ways to activate p53. *Oncogene* **26**, 1306-1316 (2007).

24. E. Gottlieb, K. H. Vousden, p53 regulation of metabolic pathways. *Cold Spring Harb Perspect Biol* **2**, a001040 (2010).

25. T. J. Humpton, K. H. Vousden, Regulation of Cellular Metabolism and Hypoxia by p53. *Cold Spring Harb Perspect Med* **6**, (2016).

26. I. A. Olovnikov, J. E. Kravchenko, P. M. Chumakov, Homeostatic functions of the p53 tumor suppressor: regulation of energy metabolism and antioxidant defense. *Semin Cancer Biol* **19**, 32-41 (2009).

27. P. Jiang, W. Du, A. Mancuso, K. E. Wellen, X. Yang, Reciprocal regulation of p53 and malic enzymes modulates metabolism and senescence. *Nature* **493**, 689-693 (2013).

28. R. G. Jones, D. R. Plas, S. Kubek, M. Buzzai, J. Mu, Y. Xu, M. J. Birnbaum, C. B. Thompson, AMP-activated protein kinase induces a p53-dependent metabolic checkpoint. *Mol Cell* **18**, 283-293 (2005).

29. O. D. Maddocks, C. R. Berkers, S. M. Mason, L. Zheng, K. Blyth, E. Gottlieb, K. H. Vousden, Serine starvation induces stress and p53-dependent metabolic remodelling in cancer cells. *Nature* **493**, 542-546 (2013).

30. J. L. Chen, J. E. Lucas, T. Schroeder, S. Mori, J. Wu, J. Nevins, M. Dewhirst, M. West, J. T. Chi, The genomic analysis of lactic acidosis and acidosis response in human cancers. *PLoS Genet* **4**, e1000293 (2008).

31. C. C. Fjeld, W. T. Birdsong, R. H. Goodman, Differential binding of NAD+ and NADH allows the transcriptional corepressor carboxyl-terminal binding protein to serve as a metabolic sensor. *Proc Natl Acad Sci U S A* **100**, 9202-9207 (2003).

32. P. Tsvetkov, G. Asher, V. Reiss, Y. Shaul, L. Sachs, J. Lotem, Inhibition of NAD(P)H:quinone oxidoreductase 1 activity and induction of p53 degradation by the natural phenolic compound curcumin. *Proc Natl Acad Sci U S A* **102**, 5535-5540 (2005).

33. K. Shigemori, T. Ishizaki, S. Matsukawa, A. Sakai, T. Nakai, S. Miyabo, Adenine nucleotides via activation of ATP-sensitive K+ channels modulate hypoxic response in rat pulmonary artery. *Am J Physiol* **270**, L803-809 (1996).

34. L. M. Bergman, J. P. Blaydes, C-terminal binding proteins: emerging roles in cell survival and tumorigenesis. *Apoptosis* **11**, 879-888 (2006).

35. G. Chinnadurai, The transcriptional corepressor CtBP: a foe of multiple tumor suppressors. *Cancer Res* **69**, 731-734 (2009).

36. P. Balasubramanian, L. J. Zhao, G. Chinnadurai, Nicotinamide adenine dinucleotide stimulates oligomerization, interaction with adenovirus E1A and an intrinsic dehydrogenase activity of CtBP. *FEBS Lett* **537**, 157-160 (2003).

37. V. Kumar, J. E. Carlson, K. A. Ohgi, T. A. Edwards, D. W. Rose, C. R. Escalante, M. G. Rosenfeld, A. K. Aggarwal, Transcription corepressor CtBP is an NAD(+)-regulated dehydrogenase. *Mol Cell* **10**, 857-869 (2002).

38. M. Nardini, S. Spano, C. Cericola, A. Pesce, A. Massaro, E. Millo, A. Luini, D. Corda, M. Bolognesi, CtBP/BARS: a dual-function protein involved in transcription co-repression and Golgi membrane fission. *EMBO J* **22**, 3122-3130 (2003).

39. L. J. Zhao, M. Kuppuswamy, S. Vijayalingam, G. Chinnadurai, Interaction of ZEB and histone deacetylase with the PLDLS-binding cleft region of monomeric C-terminal binding protein 2. *BMC Mol Biol* **10**, 89 (2009).

40. C. Bhambhani, J. L. Chang, D. L. Akey, K. M. Cadigan, The oligomeric state of CtBP determines its role as a transcriptional co-activator and co-repressor of Wingless targets. *EMBO J* **30**, 2031-2043 (2011).

41. L. J. Di, J. S. Byun, M. M. Wong, C. Wakano, T. Taylor, S. Bilke, S. Baek, K. Hunter, H. Yang, M. Lee, C. Zvosec, G. Khramtsova, F. Cheng, C. M. Perou, C. R. Miller, R. Raab, O. I. Olopade, K. Gardner, Genome-wide profiles of CtBP link metabolism with genome stability and epithelial reprogramming in breast cancer. *Nature communications* **4**, 1449 (2013).

42. S. Paliwal, R. C. Kovi, B. Nath, Y. W. Chen, B. C. Lewis, S. R. Grossman, The alternative reading frame tumor suppressor antagonizes hypoxia-induced cancer cell migration via interaction with the COOH-terminal binding protein corepressor. *Cancer Res* **67**, 9322-9329 (2007).

43. A. H. Mirnezami, S. J. Campbell, M. Darley, J. N. Primrose, P. W. M. Johnson, J. P. Blaydes, Hdm2 recruits a hypoxia sensitive co-repressor to negatively regulate p53-dependent transcription. *Curr. Biol.* **13**, 1234-1239 (2003).

44. L. M. Bergman, C. N. Birts, M. Darley, B. Gabrielli, J. P. Blaydes, CtBPs promote cell survival through the maintenance of mitotic fidelity. *Mol. Cell. Biol.* **29**, 4539-4551 (2009).

45. L. J. Reitzer, B. M. Wice, D. Kennell, Evidence that glutamine, not sugar, is the major energy source for cultured HeLa cells. *J Biol Chem* **254**, 2669-2676 (1979).

46. K. Birsoy, R. Possemato, F. K. Lorbeer, E. C. Bayraktar, P. Thiru, B. Yucel, T. Wang, W. W. Chen, C. B. Clish, D. M. Sabatini, Metabolic determinants of cancer cell sensitivity to glucose limitation and biguanides. *Nature* **508**, 108-112 (2014).

47. C. N. Birts, S. K. Nijjar, C. A. Mardle, F. Hoakwie, P. J. Duriez, J. P. Blaydes, A. Tavassoli, A cyclic peptide inhibitor of C-terminal binding protein dimerization links metabolism with mitotic fidelity in breast cancer cells. *Chem Sci* **4**, 3046-3057 (2013).

48. A. Banerjee, P. Arvinrad, M. Darley, S. A. Laversin, R. Parker, M. J. J. Rose-Zerilli, P. A. Townsend, R. I. Cutress, S. A. Beers, F. D. Houghton, C. N. Birts, J. P. Blaydes, The effects of restricted glycolysis on stem-cell like characteristics of breast cancer cells. *Oncotarget* **9**, 23274-23288 (2018).

49. A. Loewer, E. Batchelor, G. Gaglia, G. Lahav, Basal dynamics of p53 reveal transcriptionally attenuated pulses in cycling cells. *Cell* **142**, 89-100 (2010).

50. M. Fischer, Census and evaluation of p53 target genes. *Oncogene* **36**, 3943-3956 (2017).

51. R. Lev Bar-Or, R. Maya, L. A. Segel, U. Alon, A. J. Levine, M. Oren, Generation of oscillations by the p53-Mdm2 feedback loop: a theoretical and experimental study. *Proc Natl Acad Sci U S A* **97**, 11250-11255. (2000).

52. F. X. Yu, R. P. Dai, S. R. Goh, L. Zheng, Y. Luo, Logic of a mammalian metabolic cycle: an oscillated NAD+/NADH redox signaling regulates coordinated histone expression and S-phase progression. *Cell Cycle* **8**, 773-779 (2009).

53. C. E. Cano, J. Gommeaux, S. Pietri, M. Culcasi, S. Garcia, M. Seux, S. Barelier, S. Vasseur, R. P. Spoto, M. J. Pebusque, N. J. Dusetti, J. L. Iovanna, A. Carrier, Tumor protein 53-induced nuclear protein 1 is a major mediator of p53 antioxidant function. *Cancer Res* **69**, 219-226 (2009).

54. Y. L. Li, J. T. Chang, L. Y. Lee, K. H. Fan, Y. C. Lu, Y. C. Li, C. H. Chiang, G. R. You, H. Y. Chen, A. J. Cheng, GDF15 contributes to radioresistance and cancer stemness of head and

neck cancer by regulating cellular reactive oxygen species via a SMAD-associated signaling pathway. *Oncotarget* **8**, 1508-1528 (2017).

55. N. M. Gruning, D. Du, M. A. Keller, B. F. Luisi, M. Ralser, Inhibition of triosephosphate isomerase by phosphoenolpyruvate in the feedback-regulation of glycolysis. *Open biology* **4**, 130232 (2014).

56. C. N. Birts, L. M. Bergman, J. P. Blaydes, CtBPs promote mitotic fidelity through their activities in the cell nucleus. *Oncogene* **30**, 1272-1280 (2011).

57. O. D. Maddocks, K. H. Vousden, Metabolic regulation by p53. *J Mol Med (Berl)* **89**, 237-245 (2011).

58. A. Phillips, A. Teunisse, S. Lam, K. Lodder, M. Darley, M. Emaduddin, A. Wolf, J. Richter, J. de Lange, M. Verlaan-de Vries, K. Lenos, A. Bohnke, F. Bartel, J. P. Blaydes, A. G. Jochemsen, HDMX-L is expressed from a functional p53-responsive promoter in the first intron of the HDMX gene and participates in an autoregulatory feedback loop to control p53 activity. *J Biol Chem* **285**, 29111-29127 (2010).

59. D. P. Lane, Cancer. p53, guardian of the genome. *Nature* **358**, 15-16 (1992).

60. M. Hollstein, D. Sidransky, B. Vogelstein, C. C. Harris, p53 mutations in human cancers. *Science* **253**, 49-53 (1991).

61. D. Wynford-Thomas, J. Blaydes, The influence of cell context on the selection pressure for p53 mutation in human cancer. *Carcinogenesis* **19**, 29-36 (1998).

62. D. H. Christiansen, M. K. Andersen, J. Pedersen-Bjergaard, Mutations with loss of heterozygosity of p53 are common in therapy-related myelodysplasia and acute myeloid leukemia after exposure to alkylating agents and significantly associated with deletion or loss of 5q, a complex karyotype, and a poor prognosis. *J Clin Oncol* **19**, 1405-1413 (2001).

63. A. Chiarugi, C. Dolle, R. Felici, M. Ziegler, The NAD metabolome--a key determinant of cancer cell biology. *Nat Rev Cancer* **12**, 741-752 (2012).

64. E. Z. Macosko, A. Basu, R. Satija, J. Nemesh, K. Shekhar, M. Goldman, I. Tirosh, A. R. Bialas, N. Kamitaki, E. M. Martersteck, J. J. Trombetta, D. A. Weitz, J. R. Sanes, A. K. Shalek, A. Regev, S. A. McCarroll, Highly Parallel Genome-wide Expression Profiling of Individual Cells Using Nanoliter Droplets. *Cell* **161**, 1202-1214 (2015).

**Acknowledgments:** Peredox-encoding plasmids were made available by G. Yellen (Harvard Medical School). **Funding:** Funding from Breast Cancer Now (2014NovPR341 and 2010NovPR12) and Cancer Research UK (C34999/A18087). Medical Research Council, UK, (MC_PC_15078) and a University of Southampton Institute For Life Sciences fellowship (J.W.) supported the establishment of single-cell mRNA sequencing. C.N.B. is now an Against Breast Cancer-funded lecturer at the School of Biological Sciences, University of Southampton. **Author contributions:** Conceptualization and methodology: J.P.B. and C.N.B.; Investigation and analysis: C.N.B., A.B., M.D., C.D., S.K.N., R.P., M.J.J.R.-Z., J.W., and J.P.B.; Writing, original draft: J.P.B. and C.N.B.; Writing, review and editing: J.P.B., C.N.B., A.B., A.T., J.W., and M.J.J.R.-Z.; Funding acquisition: J.P.B., C.N.B., and A.T. **Competing interests:** J.P.B. has served as a member of the Scientific Advisory Board of Breast Cancer Now. The other authors declare that they have no competing interests. **Data and materials availability:** The datasets generated analyzed during the current study are available in the gene expression omnibus repository (https://www.ncbi.nlm.nih.gov/geo/) with the identifier GSE115869. All data needed to evaluate the conclusions in the paper are present in the paper or the Supplementary Materials.

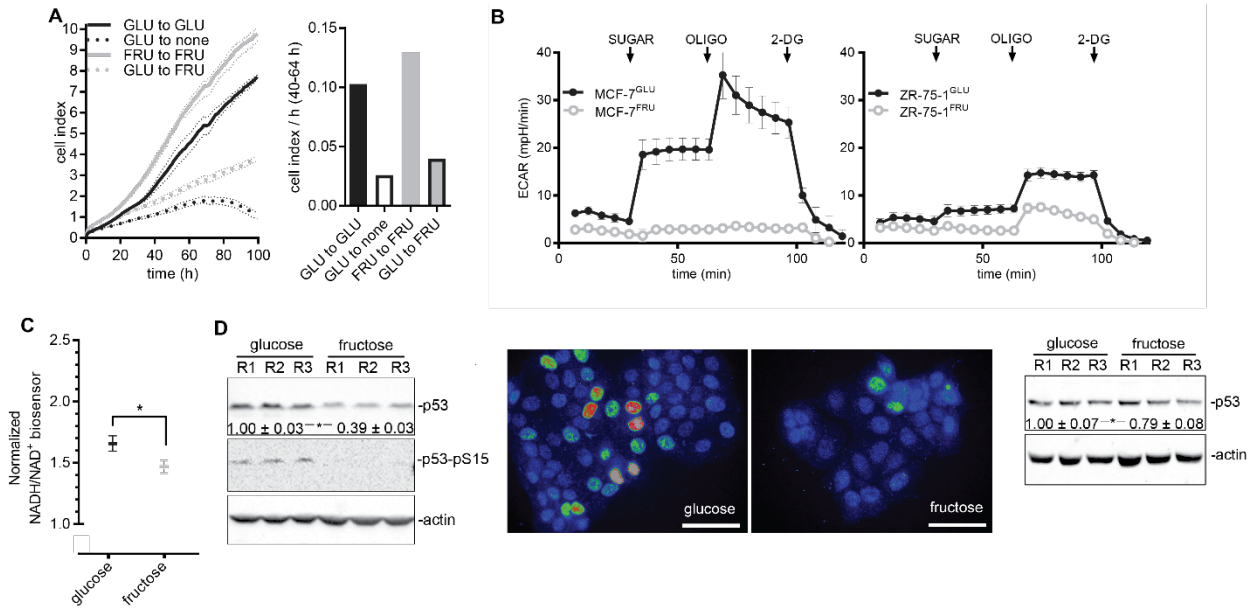


**Fig. 1. p53 protein abundance is increased in glycolytic cells.** (**A**) MCF-7$^{GLU}$ and MCF-7$^{FRU}$ cells had their culture medium replaced with one containing the indicated sugar and then were analyzed for proliferation using xCELLigence. Left: Cell index showing cell proliferation from 1 to 100 hours after plating. Data are means ± range of at least two experiments. Right: Proliferation rates (40 to 100 hours). Data are representative of two experiments. (**B**) Glucose or fructose-adapted breast cancer cells (as indicated) were analyzed for rates of glycolysis-dependent extracellular acidification (ECAR) using a Seahorse XF96. Initial readings were taken in medium lacking sugar, and then ports were injected with the sugar to which the cells had been adapted. Data are means ± SEM of four technical replicates. Data are representative of two experiments. (**C**) Determination of the NADH/NAD$^+$ ratios of glucose- and fructose-cultured MCF-7 cells by Peredox biosensor analysis. Data are means ± SEM of at least 80 cells from a representative of two experiments and were analyzed by unpaired *t* test. Calibration is shown in fig. S1C. (**D**) Left: MCF-7 cells adapted to the indicated sugar were lysed and subjected to Western blotting analysis with antibodies specific for the indicated targets. Numbers indicate the mean ± SEM of the normalized p53 band intensities from three experiments (R1 to R3) and were analyzed by paired *t* test. Middle: Immunofluorescence staining of p53 in MCF-7$^{GLU}$ and MCF-7$^{FRU}$ cells. A rainbow lookup table demonstrates p53 staining intensity (blue/low → red/high, ~15-fold maximum range between cells). Scale bar, 50 µm. Right: ZR-75-1 cells adapted to the indicated sugar were lysed and subjected to Western blotting analysis with antibodies specific for the indicated targets. Numbers indicate the mean ± SEM of the normalized p53 band intensities from three experiments and were analyzed by paired *t* test. p53-pSer$^{15}$ was undetectable in these cells.

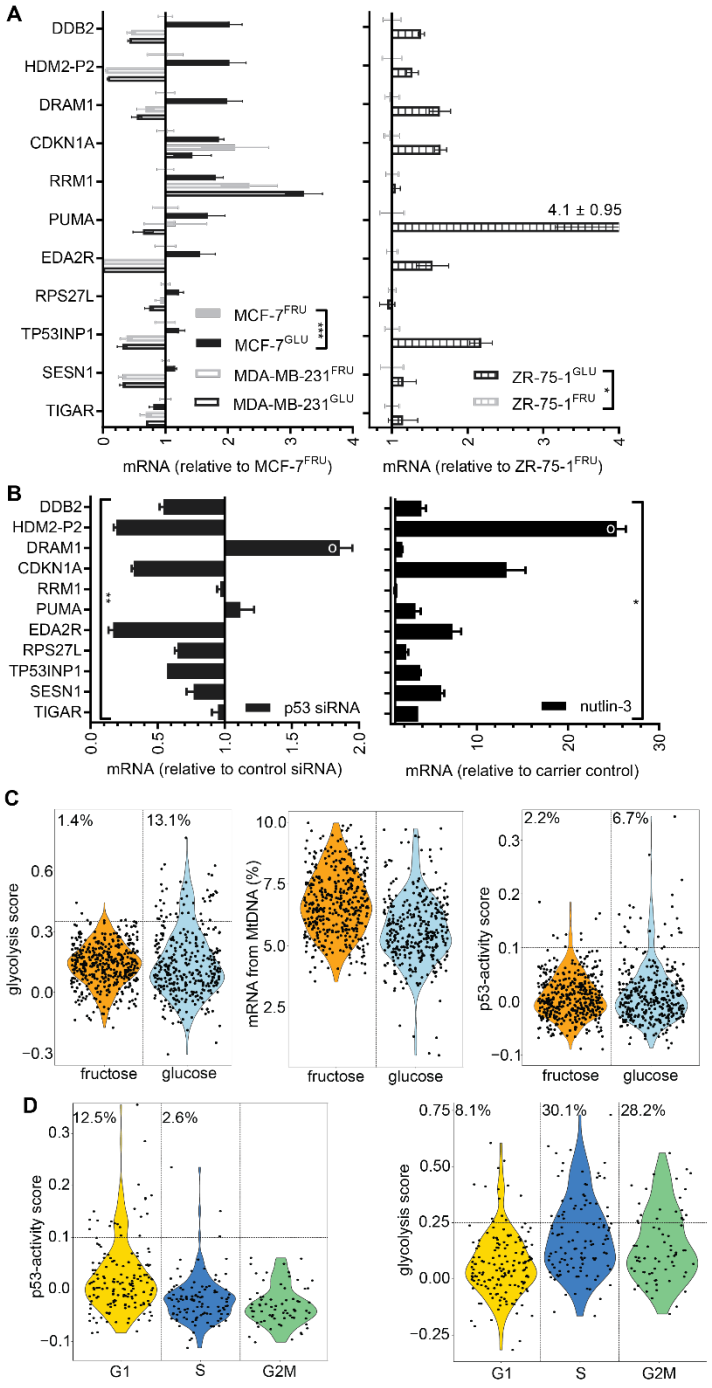


**Fig. 2. Glycolysis promotes p53-dependent gene expression.** (**A**) RT-qPCR analysis of the expression of a panel of known p53-responsive genes in glucose- and fructose-cultured cells. Data are means ± SEM of three experiments. (**B**) mRNAs were extracted from MCF-7 cells in which p53 had been either suppressed by p53-specific siRNA (72 hours after transfection; data are means ± SEM of three experiments) or induced by treatment with 5 μM nutlin-3 for 24 hours (data are means ± SEM of three experiments), o, outlier. (**C** and **D**) Whole-transcriptome, single-cell mRNA-seq was performed on MCF-7$^{GLU}$ and MCF-7$^{FRU}$ cells. Data are combined from three experiments. (C) Violin plots comparing MCF-7$^{GLU}$ cells with MCF-7$^{FRU}$ cells in terms of glycolysis gene expression score (left), percentage of all mRNA transcripts that are derived from mitochondrial DNA (middle), and p53-activity gene expression score (right). (D) Analysis of MCF-7$^{GLU}$ cells alone. Violin plots of p53-activity score (left) and glycolysis score (right), according to assigned cell cycle phase. The percentage of cells in each phase with a score greater than the threshold value is indicated.

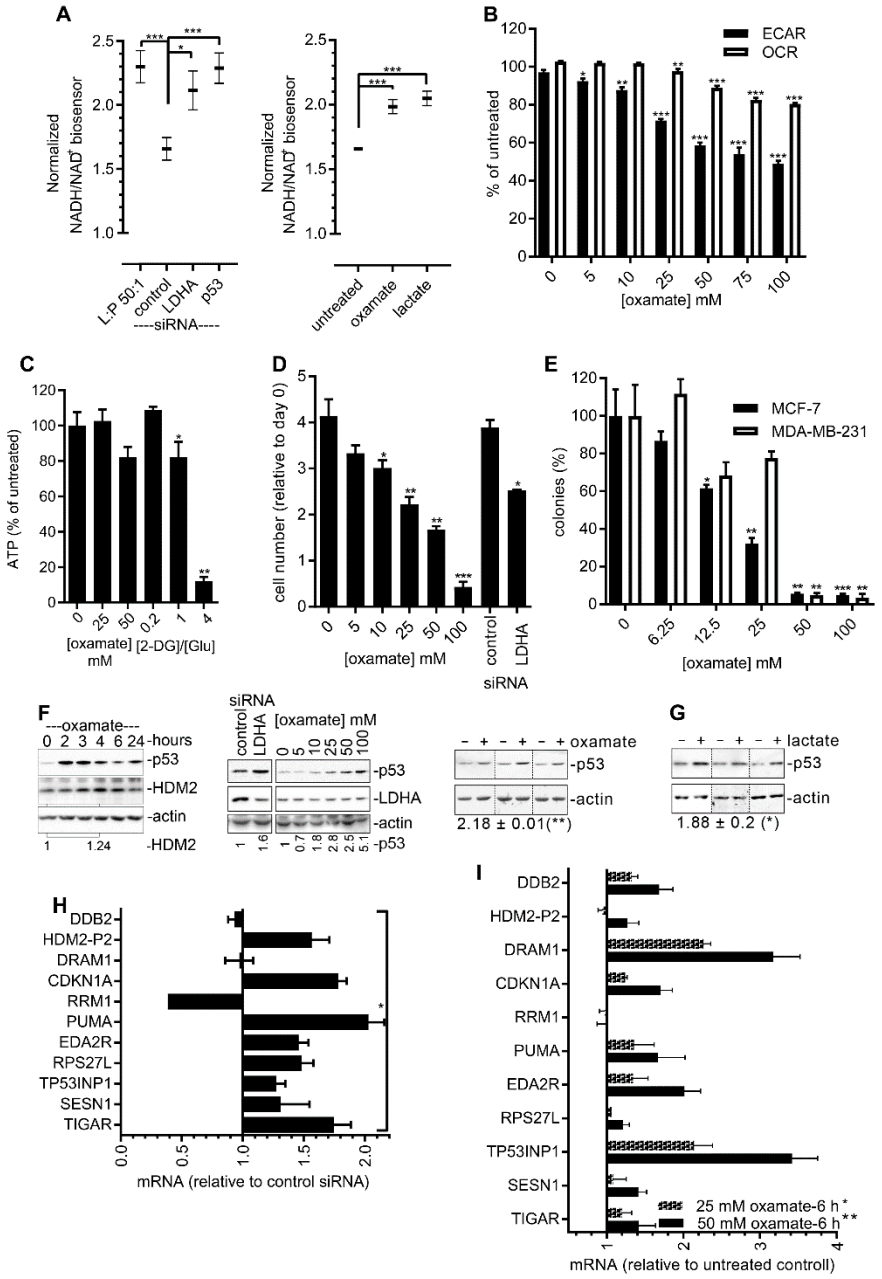


**Fig. 3. Inhibition of LDH activates p53.** (**A**) NADH/NAD$^+$ ratios in MCF-7$^{GLU}$ cells were measured using the Peredox biosensor. Left: Forty-eight hours after transfection with the indicated siRNAs. Data from control siRNA–transfected cells 6 min after the addition of 50 mM lactate to the medium (L:P 50:1) are included as a positive control. Right: No transfection with siRNA. The cells were imaged as described earlier, and 6 min after the addition of medium containing 50 mM sodium oxamate or 50 mM lactate, the fold change in green/red ratio was determined. Control, medium alone added. Data in both panels are means ± SEM of at least 35 cells from a representative of two or more experiments and were analyzed by unpaired *t* test. (**B**) The effect of increasing concentrations of sodium oxamate on ECAR and OCR in MCF-7 cells was determined using Seahorse XF96. Data are means ± SEM of four experiments. Data were analyzed by unpaired *t* test and compared to the 0 mM control. (**C**) ATP was measured in MCF-7$^{GLU}$ cells in 25 mM glucose (Glu) 2 hours after the initiation of treatment with oxamate or 2-deoxyglucose (2-DG). Data are means ± SEM of three experiments and were analyzed by paired *t* test compared to the 0 mM control. (**D**) MCF-7$^{GLU}$ cells were transfected with the indicated siRNAs or were continuously exposed to the indicated concentrations of sodium oxamate, and the effect on proliferation was determined at 72 hours. Data are means ± SEM of three experiments and were analyzed by unpaired *t* test compared to either the 0 mM oxamate condition or to the control siRNA. (**E**) Cells were plated as single cells at a low density and exposed to the indicated concentrations of sodium oxamate for 10 days before colonies were counted. Data are means ± SEM of three experiments and were analyzed by unpaired t-test and compared to the 0 mM oxamate condition. (**F**) MCF-7$^{GLU}$ cells. Left: Western blotting analysis of p53 and HDM2 protein abundance during exposure to 50 mM sodium oxamate for the indicated times. Data are representative of two experiments. Middle: Western blotting analysis of p53 protein abundance after 2 hours of exposure to the indicated concentrations of sodium oxamate or 48 hours after transfection with control of LDHA-specific siRNA. Right: Western blotting analysis of p53 abundance in three biological replicates (separated by vertical dotted lines) after 2 hours of exposure to 50 mM sodium oxamate. Numbers under the blot indicate the mean ± SEM of the relative intensity of the p53 bands in the oxamate-treated cells compared to that in the untreated cells, which was set at 1. Data were analyzed by paired *t* test. (**G**) MCF-7$^{GLU}$ cells (three biological replicates separated by vertical dotted lines) were cultured as described in (A) for 6 hours in the absence or presence of 50 mM lactate before being analyzed by Western blotting for p53 abundance. Numbers under the blot indicate the mean ± SEM of the relative intensity of the p53 bands in the lactate-treated cells compared to that in the untreated cells, which was set at 1. Data were analyzed by paired *t* test. (**H**) RT-qPCR analysis of mRNAs extracted from MCF-7$^{GLU}$ cells in which LDHA was knocked down by LDHA-specific siRNA. Samples were analyzed 72 hours after transfection. Data are means ± SEM of three experiments. Knockdown of LDHA protein by the specific siRNA is shown in fig. S3. (**I**) RT-qPCR analysis of mRNAs extracted from MCF-7$^{GLU}$ cells in which LDH was inhibited by treatment with the indicated concentrations of sodium oxamate for 6 hours. Data are means ± SEM of three experiments.

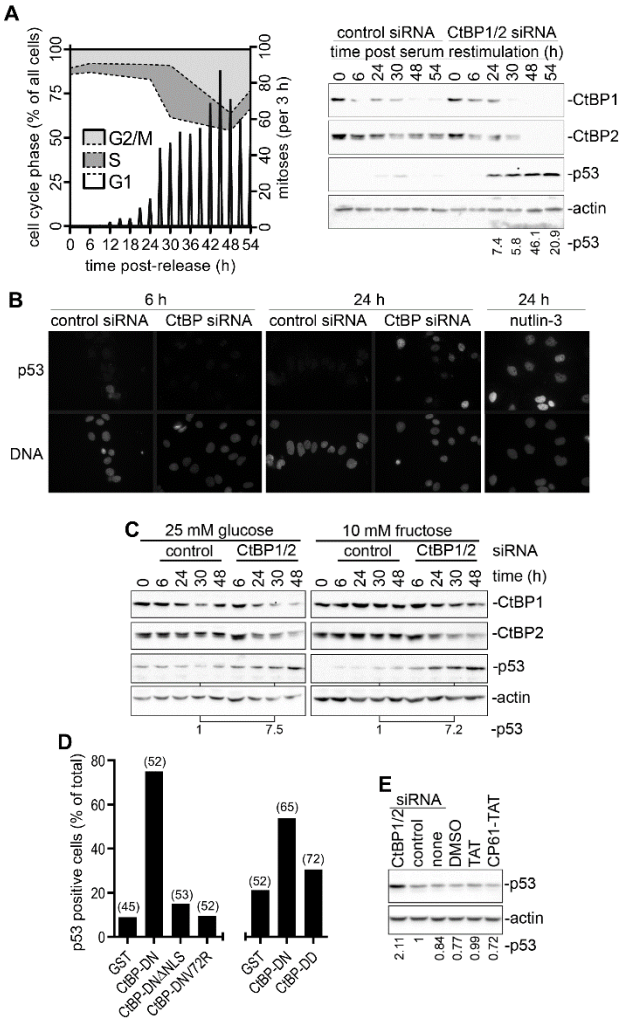


**Fig. 4. CtBPs are required to prevent the accumulation of p53 protein in proliferating cells.** (**A**) MCF-7 cells were synchronized by serum starvation for 48 hours and then transfected with control of CtBP1/2-specific siRNAs at the point of re-stimulation with serum. Left: Cell cycle phase in the control siRNA–transfected cells was determined by propidium iodide flow cytometry (left axis), whereas mitotic events were determined by time-lapse video microscopy (right axis). Right: Western blotting of the indicated samples for CtBP1, CtBP2, and p53. Blots are representative of three experiments. Quantification shows the effect (fold-increase) of CtBP1/2-specific siRNA on p53 abundance compared to that of control siRNA at the equivalent times. (**B**) MCF-7 cells were transfected and re-stimulated with serum as described in (A) and p53 was detected by immunofluorescence staining. Cells exposed to 5 μM nutlin-3 are included for comparison. Images are representative of two experiments. (**C**) MCF-$7^{GLU}$ and MCF-$7^{FRU}$ cells transfected with the indicated siRNAs were analyzed by Western blotting at the indicated times after culture under the indicated conditions. Blots are from a single experiment. Quantification of the effect of CtBP1/2-specific siRNA versus control siRNA on p53 abundance at the 30-hour time point is shown . (**D**) At the point of release from serum starvation MCF-7 cells were microinjected with the indicated GST miniproteins. Twenty-four hours later, p53 in the injected cells was determined by immunofluorescence staining and the percentages of p53-positive cells were determined. The numbers of microinjected cells analyzed are shown in parentheses. The broken x-axis indicates that the results are from independently controlled experiments (**E**) MCF-7 cells were treated with CP61-TAT, TAT only, or DMSO for 48 hours before being subjected to Western blotting analysis for p53. Cells transfected with CtBP1/2-specific siRNA are included as a positive control. Blots are representative of three experiments.

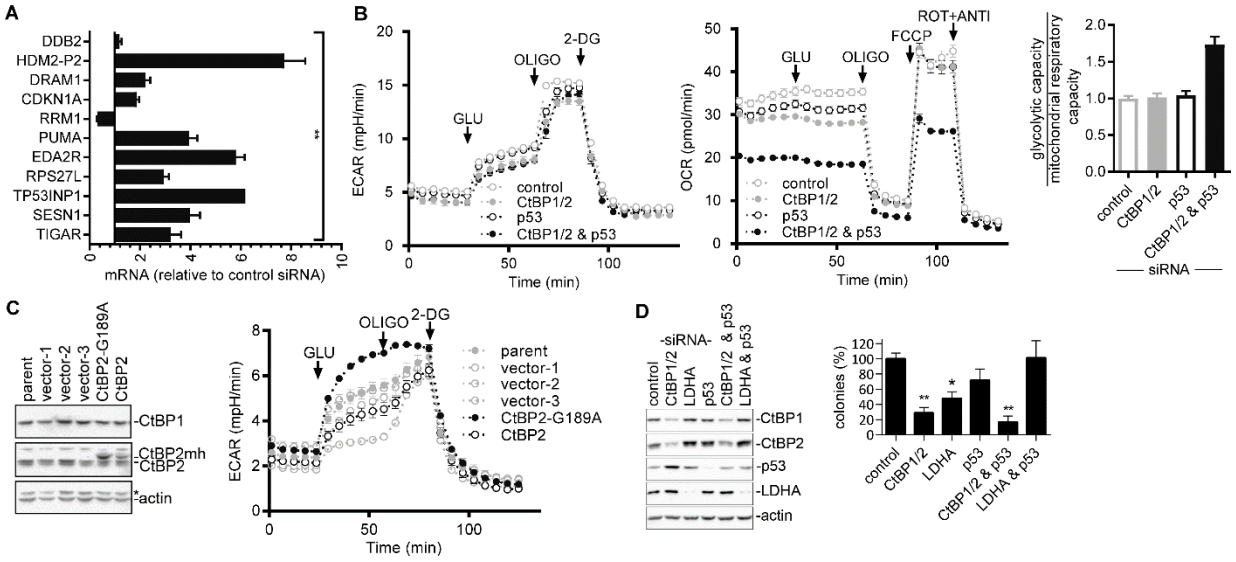


**Fig. 5. Functional consequences of the regulation of p53 by CtBPs.** (**A**) mRNAs were extracted from MCF-7 cells 72 hours after they had been transfected with control or CtBP1/2-specific siRNAs. Data are means ± SEM of three experiments. Knockdown of CtBP proteins by the specific siRNA is shown in fig. S3. (**B**) MCF-7 cells were transfected with the indicated siRNAs. Forty-eight hours later, the effects on ECAR (left) and OCR (middle) were determined using the Seahorse XF96 instrument. Data are means ± SEM of five technical replicates and are representative of two experiments. Right: The ratio of glycolytic capacity to mitochondrial respiratory capacity. (**C**) MCF-7 cells were stably transfected with empty vector or with plasmids encoding CtBP2 or CtBP2$^{G189A}$ and individual clones were isolated. Left: Cells were analyzed by Western blotting with antibodies against the indicated proteins. Blots are representative of two or more experiments. Right: Glycolytic ECAR was determined by Seahorse XF96. (**D**) MCF-7 cells were transfected with the indicated siRNAs and then analyzed 48 hours later. Left: Western blotting analysis of the indicated proteins. Blots are representative of three experiments. Right: Equal numbers of cells were plated at low density for colony-forming assays. Colonies were counted 10 days later. Data are means ± SEM of three experiments and were analyzed by Fisher's LSD test.

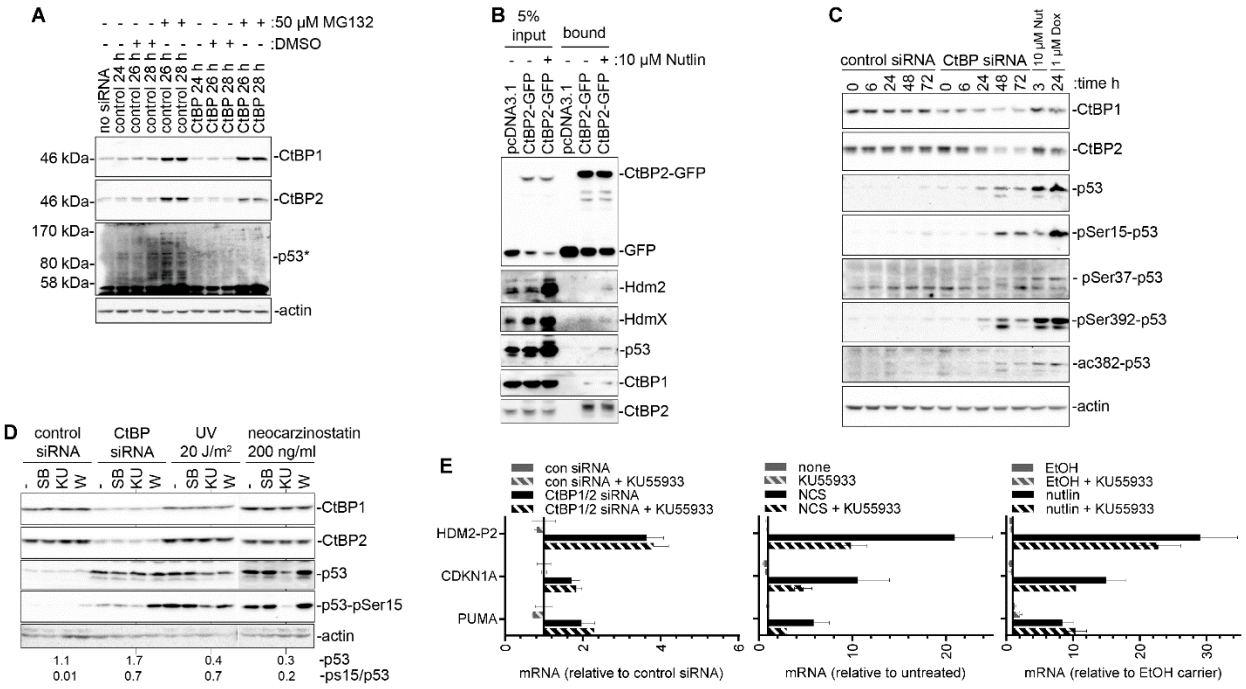


**Fig. 6. Mechanisms of regulation of p53 by CtBPs.** (**A**) MCF-7 cells were serum-starved for 48 hours transfected with the indicated siRNAs at the point of serum re-stimulation, and then treated with MG132 or DMSO 24 hours later. Cells were lysed and analyzed by Western blotting at the indicated times after serum re-stimulation. The asterisk indicates the non-ubiquitylated p53 signal is overexposed to enable visualization of the ubiquitylated p53 bands. Blots are representative of two experiments. (**B**) MCF-7 cells were transfected with the indicated plasmids together with pEGFP-N1, treated with or without 10 μM nutlin-3, and protein complexes were analyzed by GFP-Trap immunoprecipitation. Blots are representative of two experiments. (**C**) MCF-7 cells were transfected with the indicated siRNAs at the point of release from 48 hours of serum-starvation. Samples were prepared for Western blotting at the indicated times after release. Nutlin and doxorubicin were included as positive controls for p53 induction and modification. Quantification of the blots is shown in fig. S7. (**D**) MCF-7 cells were treated with 2 μM SB202190, 10 μM KU55933, or 5 μM wortmannin for 4 hours either 48 hours after transfection with the indicated siRNAs or in the presence of neocarzinostatin (200 ng/ml) or exposure to 20 J/m$^2$ UV-C. Proteins were then analyzed by Western blotting. Quantification shows the effect of KU55933 on both p53 abundance and the p53-Ser$^{15}$/p53 ratio under each treatment condition. Blots are representative of three experiments. The dotted vertical line indicates noncontiguous blots. (**E**) MCF-7 cells were transfected with control or CtBP1/2-specific siRNA. Forty-eight hours later, the cells were treated with 10 μM KU55933 for a further 24 hours. MCF-7 cells pretreated with 10 μM KU55933 for 24 hours were treated with neocarzinostatin (200 ng/ml) or 10 μM nutlin-3 for a further 4 hours before being harvested and being subjected to RT-qPCR of the relative abundances of the indicated mRNAs. Data are means ± SD of two experiments.

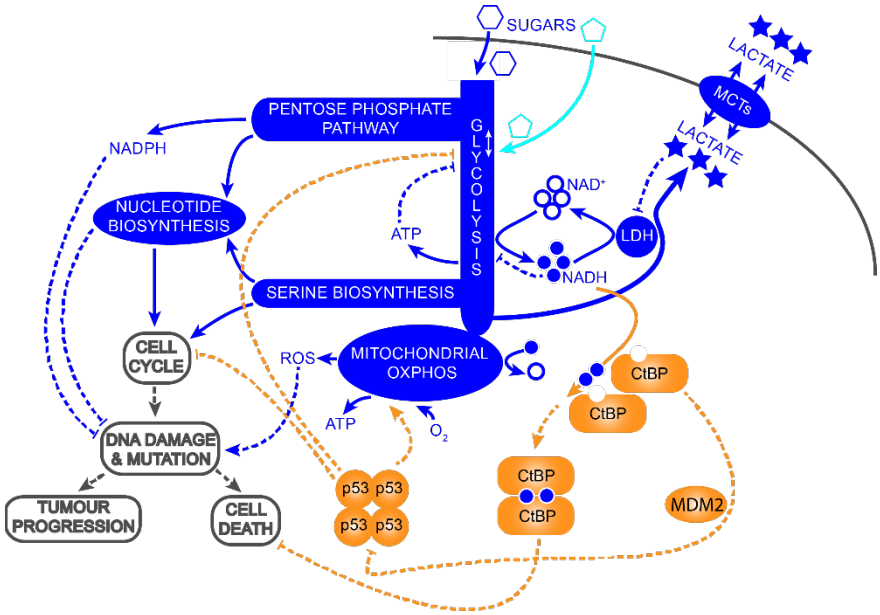


**Fig. 7. Model for the role of the NADH-CtBP-p53 pathway in the regulation of glycolytic homeostasis.** Primary metabolic pathways are shown in blue (fructose model is in cyan), cellular phenotypes are in gray, and the CtBP-p53 pathway in shown in orange. Solid lines show metabolic reactions, whereas dashed lines show regulatory relationships. Regeneration of $NAD^+$ from GAPDH-generated NADH by the mitochondrial electron transport chain is reduced by decreased $O_2$ concentrations and increased by ATP generation through glycolysis. The ability of LDH to regenerate $NAD^+$ is linked to rates of lactate export, which are inhibited by high tumor lactate concentrations. Oncogenic mutations drive both cell proliferation and increased rates of glycolysis for the synthesis of anabolic metabolites. The biochemical limitation of glycolysis due to an increased NADH:$NAD^+$ ratio may lead to an imbalance between metabolic demand and supply, resulting in cellular damage. Sensing of this ratio by CtBPs, and the subsequent regulation of p53, matches metabolic demand with supply and reduces cellular damage. In the absence of functional p53, cells continue to proliferate in adverse microenvironments despite metabolic imbalances, and surviving cells acquire further mutations resulting in tumor progression.